

High-fidelity transmission of polarization encoded qubits from an entangled source over 100 km of fiber

Hannes Hübel¹, Michael R. Vanner¹, Thomas Lederer¹,
Bibiane Blauensteiner¹, Thomas Lorünser², Andreas Poppe¹,
Anton Zeilinger^{1,3}

¹*Quantum Optics, Quantum Nanophysics and Quantum Information, Faculty of Physics, University of Vienna, Boltzmannngasse 5, 1090 Vienna, Austria*

²*Austrian Research Centers GmbH - ARC, Donau-City-Str. 1, 1220 Vienna, Austria*

³*Institute for Quantum Optics and Quantum Information, Austrian Academy of Sciences, Boltzmannngasse 3, 1090 Vienna, Austria*

hannes.huebel@univie.ac.at

Abstract: We demonstrate non-degenerate down-conversion at 810 and 1550 nm for long-distance fiber based quantum communication using polarization entangled photon pairs. Measurements of the two-photon visibility, without dark count subtraction, have shown that the quantum correlations (raw visibility 89%) allow secure quantum cryptography after 100 km of non-zero dispersion shifted fiber using commercially available single photon detectors. In addition, quantum state tomography has revealed little degradation of state negativity, decreasing from 0.99 at the source to 0.93 after 100 km, indicating minimal loss in fidelity during the transmission.

© 2007 Optical Society of America

OCIS codes: (270.0270) Quantum optics; (060.0060) Fiber optics and optical communications; (999.9999) Quantum communications; (999.9999) Quantum key distribution.

References and links

1. M. Dusek, N. Lutkenhaus, and M. Hendrych, "Quantum Cryptography," *Progress in Optics* **49**, 381-454 (2006).
2. C.H. Bennett, G. Brassard, and N.D. Mermin, "Quantum cryptography without Bell's theorem," *Phys. Rev. Lett.* **68**, 557-559 (1992).
3. H. Briegel, W. Dür, J. I. Cirac, and P. Zoller, "Quantum repeaters: the role of imperfect local operations in quantum communication," *Phys. Rev. Lett.* **81**, 5932-5935 (1998).
4. R. Ursin, F. Tiefenbacher, T. Schmitt-Manderbach, H. Weier, T. Scheidl, M. Lindenthal, B. Blauensteiner, T. Jennewein, J. Perdigues, P. Trojek, B. Oemer, M. Fuerst, M. Meyenburg, J. Rarity, Z. Sodnik, C. Barbieri, H. Weinfurter, and A. Zeilinger, "Free-Space distribution of entanglement and single photons over 144 km," <http://www.arxiv.org/abs/quant-ph/0607182>.
5. I. Marcikic, H. de Riedmatten, W. Tittel, H. Zbinden, M. Legré, and N. Gisin, "Distribution of Time-Bin Entangled Qubits over 50 km of Optical Fiber," *Phys. Rev. Lett.* **93**, 180502 (2004).
6. H. Takesue, "Long-distance distribution of time-bin entanglement generated in a cooled fiber," *Opt. Express* **14**, 3453-3460 (2006).
7. C. Liang, K. F. Lee, J. Chen, and P. Kumar, "Distribution of fiber-generated polarization entangled photon-pairs over 100 km of standard fiber in OC-192 WDM environment," postdeadline paper, Optical Fiber Communications Conference (OFC2006), paper PDP35.
8. S. Sauge, M. Swillo, S. Albert-Seifried, G. B. Xavier, J. Waldebäck, M. Tengner, D. Ljunggren, A. Karlsson, "Narrowband polarization-entangled photon pairs distributed over a WDM link for qubit networks," *Opt. Express* **15**, 6926-6933 (2007).
9. D.N. Matsukevich, T. Chaneliere, S.D. Jenkins, S.Y. Lan, T.A.B. Kennedy, and A. Kuzmich, "Entanglement of Remote Atomic Qubits," *Phys. Rev. Lett* **96**, 030405 (2006).

10. A. Poppe, A. Fedrizzi, R. Ursin, H. R. Böhm, T. Lorünser, O. Maurhardt, M. Peev, M. Suda, C. Kurtsiefer, H. Weinfurter, T. Jennewein, and A. Zeilinger, "Practical quantum key distribution with polarization entangled photons," *Opt. Express* **12**, 3865-3871 (2004).
11. G. Ribordy, J. Brendel, J.D. Gautier, N. Gisin, and H. Zbinden, "Long-distance entanglement-based quantum key distribution," *Phys. Rev. A* **63**, 012309 (2000).
12. M. Pelton, P. Marsden, D. Ljunggren, M. Tenger, A. Karlsson, A. Fragemann, C. Canalias, and F. Laurell, "Bright, single-spatial-mode source of frequency non-degenerate, polarization-entangled photon pairs using periodically poled KTP," *Opt. Express* **12**, 3573-3580 (2004).
13. F. König, E.J. Mason, F.N.C. Wong, and M.A. Albota, "Efficient and spectrally bright source of polarization-entangled photons," *Phys. Rev. A* **71**, 033805 (2005).
14. P.G. Kwiat, E. Waks, A.G. White, I. Appelbaum, and P.H. Eberhard, "Ultrabright source of polarization-entangled photons," *Phys. Rev. A* **60**, R773-6 (1999).
15. D. Ljunggren, and M. Tengner, "Optimal focusing for maximal collection of narrow-band photon pairs into single-mode fibers," *Phys. Rev. A* **72**, 062301 (2005).
16. D. Ljunggren, M. Tengner, P. Marsden, and M. Pelton, "Theory and experiment of entanglement in a quasi-phase-matched two-crystal source," *Phys. Rev. A* **73**, 032326 (2006).
17. J. N. Damask, *Polarization Optics in Telecommunications* (Springer 2005).
18. D.F.V. James, P.G. Kwiat, W.J. Munro, and A.G. White, "Measurement of qubits," *Phys. Rev. A* **64**, 052312 (2001).
19. Z. Hradil, "Quantum-state estimation," *Phys. Rev. A* **55**, R1561-R1564 (1997).
20. G. Vidal and R.F. Werner, "Computable measure of entanglement," *Phys. Rev. A* **65**, 032314 (2002).
21. P.G. Kwiat, S. Barraza-Lopez, A. Stefanov, and N. Gisin, "Experimental entanglement distillation and 'hidden' non-locality," *Nature* **409**, 1014-1017 (2001).
22. E. Waks, A. Zeevi, and Y. Yamamoto, "Security of quantum key distribution with entangled photons against individual attacks," *Phys. Rev. A* **65**, 052310 (2002).
23. G. Brassard, and L. Salvail, "Secret key reconciliation by public discussion," *Lecture Notes in Computer Science* **765**, 410423 (1994).
24. N. Lütkenhaus, "Security against individual attacks for realistic quantum key distribution," *Phys. Rev. A* **61**, 052304 (2000).
25. C. Liang, K. F. Lee, M. Medic, and P. Kumar, "Characterization of fiber-generated entangled photon pairs with superconducting single-photon detectors," *Opt. Express* **12**, 3573-3580 (2004).

1. Introduction

The use of quantum entanglement in combination with existing fiber telecommunication networks offers the possibility to implement long-distance quantum communication protocols like quantum key distribution (QKD) [1, 2] and applications such as quantum repeaters [3] in the future. If the existing infrastructure is used several prerequisites have to be met: Firstly, the entanglement has to be shared by at least one photon in the 1550 nm telecom band to utilize low fiber absorption. Secondly, the fidelity of the quantum correlations after transmission has to be sufficient for the detection of eavesdropping without performing post-corrections and thirdly, the detection rate of photon pairs has to be high enough for a meaningful application and also to overcome the limitation of detector dark counts.

In this work we report a high generation rate of polarization entangled photon pairs at 810 and 1550 nm by asymmetric spontaneous parametric down-conversion (SPDC) and investigations into any depolarization of the 1550 nm photon with fiber transmission by means of measurement of the two-photon visibility and quantum state tomography. This is the first time that quantum correlations have been distributed over 100 km of optical fiber sufficiently high for QKD without any post-corrections. In the QKD scheme, it is essential to attribute all measured errors to the eavesdropper and hence no background subtraction is allowed. In addition, a high detection rate of ~ 100 pairs/s after 100 km, makes our distribution scheme readily practical for long-distance quantum communication applications.

Using the polarization degree of freedom of single photons as a carrier of information has long been seen as disadvantageous in fiber transmission. Although long-distance transmission of polarization encoded qubits was successfully demonstrated in free space up to 144 km [4], birefringent effects of the fiber were believed to hinder long-distance transmission of the po-

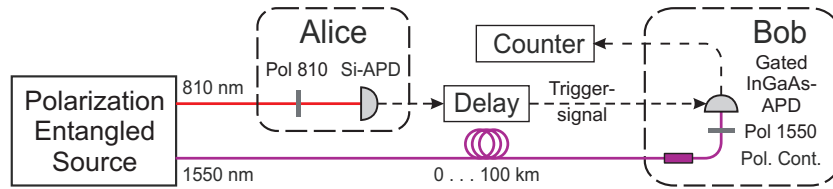


Fig. 1. (color online) Distribution and Measurement Scheme: A source of polarization entangled photon pairs produces photons at 810 and 1550 nm. The 810 nm pair-photons are polarization analyzed locally by Alice with a rotatable polarizer (Pol 810) and subsequently detected by her silicon APD (Si-APD). The partner photons at 1550 nm are transmitted to Bob via telecom fibers on spools, analyzed (Pol 1550) and detected by an InGaAs-APD. The random rotation in polarization is compensated by an electronic polarization controller (Pol.Cont.). The trigger signals are carefully matched by an electronic delay generator (Delay) to the transmission time through the fiber spools and the measured coincidence rate is displayed on a counter.

polarization state due to depolarization, mainly polarization mode dispersion (PMD). With these effects in mind, long-distance fiber transmission has been performed using time-bin entangled photons, reaching distances of 50 km [5] and 60 km [6].

Recent experiments have demonstrated polarization entanglement distribution up to 100 km [7] in fibers. However, in these experiments quantum correlation could only be shown after subtraction of background counts. In addition, the use of standard wavelength-division-multiplexing components in the quantum channel was demonstrated for polarization entangled photon pairs [7, 8] combining classical and quantum signals in a single fiber.

These results are encouraging as polarization encoded qubits can be easily produced, manipulated and detected with simple optical components. Hence the use of polarization entanglement in optical fibers brings several advantages; for instance, the construction of entanglement based QKD setups with only passive components reduces the risk of side channel attacks. Also, it allows more convenient control for interaction with atoms, thereby giving greater opportunity for the development of quantum memory and repeater devices (e.g. conversion of polarization encoded photons into atomic qubits [9]).

Our two-photon distribution and measurement scheme is depicted in Fig. 1. A source of polarization entanglement distributes photon pairs to Alice and Bob. Alice performs local polarization analysis on the 810 nm photon of the pair. The 1550 nm photon is transmitted to Bob who performs his own polarization analysis. The measured coincidences obtained by Alice and Bob can be used to characterize the shared quantum state or obtain a secret key according to the BBM92 protocol for entangled photons [2]. Such a QKD scheme has been used to demonstrate the successful distribution of secret keys in an urban environment [10].

Even though one photon of the entangled pair is measured directly, projecting the state of the other photon, the correlation carried by this photon is of quantum nature. For this reason, quantum communication protocols are made possible even if the measurements are not performed simultaneously. For example, our setup could in principle be used in a teleportation experiment, where a Bell state analysis is performed on the 810 nm photon and the to-be-teleported state. Our 1550 nm photon would then carry the teleported polarization state through the fiber. The resulting state of such a teleportation to a far away receiver is determined by the quantum correlation. The quality of these correlations, measured by quantum state tomography, are presented in this paper. In addition we investigate how the quantum correlation evolves in long distance fiber transmission and what are the principle causes.

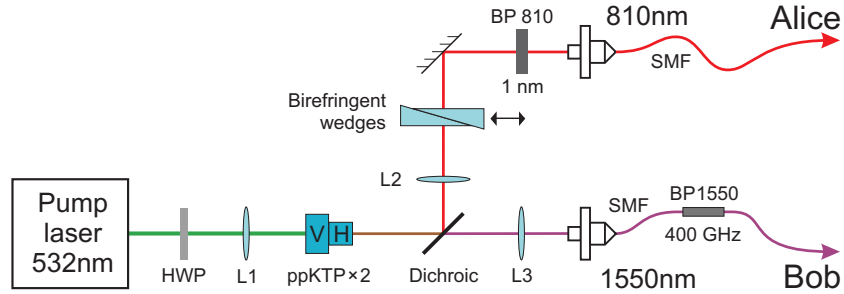


Fig. 2. (color online) Optical Setup: The solid state diode pumped laser (Pump laser 532 nm) is focused (L1) at the interface of the two periodically-poled KTP nonlinear crystals (ppKTP) for highly non-degenerate collinear down-conversion. The half-wave-plate (HWP) rotates the pump to excite the horizontal (H) and vertical (V) crystals equally. The 810 and 1550 nm photons are spatially separated (Dichroic), recollimated by lens L2 and L3 and coupled into single-mode fibers (SMF). The wavepackets are spectrally confined and matched with filters BP 1550 and BP 810. A betraying timing offset between the photons of one pair is compensated by the birefringent wedges in the 810 nm arm.

2. Source of polarization entangled photons

For long-distance fiber communication systems it is essential to have a high flux of pair generation, which we realized by producing entangled photons using spontaneous parametric down-conversion (SPDC) [11, 12, 13] in the orthogonally oriented two crystal geometry [14].

Our compact source (40×40 cm), Fig. 2, is pumped by a 532-nm-laser. For equal crystal excitation, the pump polarization is rotated to 45° with respect to the crystal axes and the beam is focussed at the boundary of two crystals. It is believed that optimal focussing is obtained when the Rayleigh range z_0 , is comparable to the individual crystal length L ($L = 4$ mm for both crystals) [15]. The beam size at the focus was measured to be 55 μm , giving a Rayleigh range of ~ 4.5 mm and hence a L/z_0 ratio of 0.9.

The two nonlinear crystals used in the source are quasi-phase matched periodically-poled KTiOPO_4 (ppKTP), with a grating spacing of 9.7 μm , which has been tailored for type-I collinear generation of an asymmetric photon pair at 810 and 1550 nm from a 532 nm pump. These wavelengths were selected because of the efficient detection at 810 nm, low fiber absorption at 1550 nm and readily available stable radiation sources at 532 nm. The crystals are housed in a temperature controlled copper mount, heated to approximately 65 °C. Varying the temperature allows wavelength tuning for collinear emission. Each ppKTP crystal produces a pair with an intrinsic bandwidth of 800 GHz, which was reduced to 400 GHz with filters BP 810 and BP 1550 to minimize chromatic dispersion.

If the down-conversion processes in the two crystals with orthogonal polarizations are indistinguishable in terms of spectral, spatial and temporal degrees of freedom, the presence of a photon pair does not reveal in which crystal it was produced. The superposition of the two possible creation events gives rise to the polarization entangled state of the photon pair:

$$|\phi\rangle = \frac{1}{\sqrt{2}} (|H_{810} H_{1550}\rangle + e^{i\phi} |V_{810} V_{1550}\rangle)$$

However, chromatic dispersion between the 810 and 1550 nm photon inside the crystal leads to a temporal distinguishability between pairs generated in the two different crystals and hence loss of entanglement [16]. This was compensated by transmission through birefringent quartz wedges which also allow control of the phase in the entangled state to obtain either of the two type-I Bell states $|\Phi^\pm\rangle$.

Alice's photons are detected after 2 m of SMF fiber using a silicon avalanche photo diode (Si-APD), see Fig. 1, with an efficiency of $\sim 50\%$. An electronic trigger is sent from the Si-APD to gate an InGaAs detector (idQuantique id-200) to detect the corresponding photon at 1550 nm as a coincidence count on Bob's side. The quantum efficiency (QE) at this wavelength is in the range of 10-15%. Locally, with 32 m SMF fiber to connect Bob, we achieved the following rates of polarization entangled photon pairs:

The photon rate at Alice was around 100 kcounts/s/mW. On Bob's side, with 10 μ s of dead-time to reduce afterpulsing, 3000 counts/s/mW of coincidences were detected in either polarization modes, yielding a conditional detection probability of $\sim 3\%$ (ratio of coincidence to trigger counts). For a low pump power (2 mW) the uncorrected two-photon visibility was measured to be 99%. The visibility is a measure of the polarization correlation between the photons, a proper definition is given in section 4.2. At maximum pump power of ~ 16 mW the measured coincidences were limited to 21000 counts/s mainly due to saturation effects in the InGaAs detector (limited gate rate of 4 MHz). The degree of entanglement decreases at higher power levels due to multi pair emission (production of uncorrelated pairs within the gate time) leading to a reduced visibility of 97%. All subsequent measurements were performed at the maximum power level.

3. Long-distance fiber transmission

To determine the robustness of polarization correlations in long-distance fiber transmission we used the arrangement depicted in Fig. 1. Since detector dark counts are the limiting factor in long-distance experiments, the detector bias was reduced to optimize the signal to noise ratio as represented by $\frac{QE}{\text{darkcounts}}$. An optimum was found for a reduced overbias voltage corresponding to $QE = 6\%$ with a dark count rate of $\sim 3 \times 10^{-6}$ within each gate opening time. To further reduce the influence of dark counts, all measurements were performed at the smallest possible gate width of 1.5 ns on the InGaAs detector. It was therefore important to minimize chromatic dispersion (CD) so that the temporal broadening of the photon (τ_P) was smaller than the applied gate window. The temporal broadening (τ_P) due to chromatic dispersion (CD) is given by: $\tau_P = CD \cdot \lambda_{1550} \cdot L$, where λ_{1550} is the spectral width of the 1550 photon in nm and L is the fiber length in km.

For the long-distance measurements we used two types of fiber: Standard single-mode fibers (telecom standard: ITU-T G.562) with $CD = 18$ ps/nm/km and non-zero dispersion shifted (NZDS) fibers (ITU-T G.565) with $CD \approx 5$ ps/nm/km. For an initial $\lambda_{1550} = 3.2$ nm, CD would broaden the photon wavepacket to $\tau_P = 5$ and 1.5 ns after $L = 100$ km for standard and NZDS fibers, respectively. Standard fibers are therefore inadequate to be used for long distance transmission. The first set (set I) of our investigations consisted of NZDS fibers with individual spool lengths of 6.3 and 12.6 km which could be concatenated (using FC/PC connectors) to give a total length of 63 km and a τ_P of 1 ns. To reach longer distances, we added two spools of standard fiber (12.6 km each) totaling 88.2 km and resulting in an additional CD spread of 1.5 ns (total τ_P of 2.5 ns). For measurements over even longer distances we had a second set (set II), consisting of two 50.4 km spools of NZDS fiber spliced together giving a total transmission distance of 100.8 km and a τ_P of 1.5 ns, the size of the gate window.

To gate the InGaAs detector an electronic delay generator was used to provide delays up to 500 μ s (for 101 km), where fine tuning by 0.2 ns increments was provided using the internal delay generator of the detector. Standard delay generators suffer from the problem that only one pulse at a time can be processed, resulting in a decreased processing rate as the delay increases. To handle our MHz rate for long delays, we used a custom made device (dotfast-consulting).

Due to the birefringence in the fiber, the random-walk like drift in polarization over the surface of the Poincaré sphere must be compensated by Bob before making his polarization analy-

sis. Temporal phase changes in the order of $\pi/4$ per hour are typical values in the laboratory. Using an electronic in-fiber polarization controller, the coincidence counts were minimized, while the polarizers at Alice and Bob were set to $0^\circ(V)$ and $90^\circ(H)$ respectively, which insured compensation in the HV basis. In a second step the birefringent wedges, see Fig. 2, were adjusted to yield a minimal coincidence rate at $45^\circ(+)$ and $135^\circ(-)$ settings and obtain a $|\Phi^+\rangle$ state.

Birefringence in the fiber also causes more severe effects on the polarization state, in particular polarization mode dispersion (PMD). PMD is a statistical property of the fiber and can be seen as a concatenation of lossless birefringent elements [17]. Here we limit ourselves to first order PMD, described as a set of two orthogonal axis with a differential-group delay (DGD) between them. A light pulse, which is not aligned with one of the axis, will be partially projected along the fast and slow axis. The pulse is therefore split into two pulses with separation τ_{PMD} , after transmission. If τ_{PMD} is larger than the coherence time of the pulse (τ_{coh}) then the two components will temporally not overlap and the initial polarization state is destroyed. If the situation is reversed the pulse will stay together and no depolarization is caused. The DGD of a fiber is normally stated in $\text{ps}/\sqrt{\text{km}}$ with $\tau_{PMD} = \text{DGD} \cdot \sqrt{L}$, L being the length of the fiber. Since we had no means to measure the value of τ_{PMD} directly at the time of our experiment, we relied upon the manufacturers specifications: For set I the average DGD, of our spools, was around $0.07 \text{ ps}/\sqrt{\text{km}}$. Individual values of τ_{PMD} for each 6.3 km spool varied from 0.1 to 0.2 ps and between 0.2 to 0.4 ps for the 12.6 km spools. In set II, the maximum value is $0.1 \text{ ps}/\sqrt{\text{km}}$. One has to bear in mind that PMD is a highly statistical property and fluctuations in the environment can induce large changes in τ_{PMD} . So the above values can only be seen as an estimate. Nevertheless, these parameters can be used to determine the significance of PMD. The 400 GHz bandwidth of the 1550 nm photon corresponds to a coherence time of $\tau_{coh} \approx 1.6 \text{ ps}$. So for 50 km of fiber, τ_{PMD} is around 0.6 ps, smaller but still in the range of τ_{coh} . Therefore, PMD effects are expected to play a role in long distance transmission.

4. Evolution of the polarization state during transmission

4.1. Quantum state tomography

In order to quantify the effect of the fiber transmission on the polarization state, full quantum state tomography was performed at distances of 0, 25.2, 50.4, 75.6, and 100.8 km. Coincidences were recorded in 16 different settings ($HH, HV, VH, VV, H+, V+, HR, VR, +H, +V, ++, +R, RH, RV, R+$ and RR , where R is the right-circular polarization) [18] each averaged over 10 s and together with a maximum likelihood estimation [19] the density matrix was evaluated.

The real components of the measured density matrices are depicted in Fig. 3(a). The overlap (fidelity) with the pure $|\Phi^+\rangle$ state (four columns at the corners of the matrix) is large, even with the matrix obtained at 101 km. To quantitatively characterize our density matrices and to determine any depolarization of the state with increasing transmission distance we chose to use the negativity (\mathcal{N}) [20]. The negativity is a real measure of entanglement by quantifying how negative the eigenvalues of the density matrix (ρ) become after the partial transpose (ρ^T) is taken. The higher the negativity, the more entanglement is present in the system. It is defined as the absolute value of the sum of negative eigenvalues of ρ^T

$$\mathcal{N}(\rho) = \left| \sum \frac{|\lambda_i| - \lambda_i}{2} \right|, \quad (1)$$

where λ_i are the eigenvalues of ρ^T .

From \mathcal{N} we can readily compute the logarithmic negativity $E_{\mathcal{N}}$ defined as:

$$E_{\mathcal{N}}(\rho) = \log_2(2\mathcal{N} + 1) \quad (2)$$

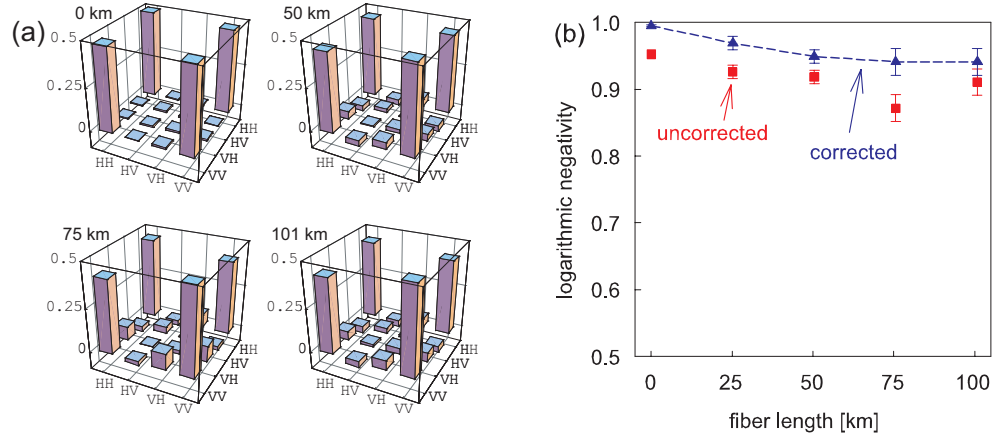


Fig. 3. (color online) (a) Real part of measured density matrices at fiber lengths of 0, 50, 75 and 101 km (raw data). The imaginary part is close to zero with no element higher than 0.09. (b) Uncorrected (■) and corrected (▲) logarithmic negativity.

The logarithmic negativity lies between zero (separable states) and one (maximal entangled states). It also bounds the maximal amount of entanglement that can be extracted (distilled) from the given state [21].

Figure 3(b) displays the values of $E_{\mathcal{N}}$ for increasing fiber lengths. $E_{\mathcal{N}}$ is calculated from the raw data and also from corrected data, where the background has been removed. The actual background was measured for each individual data point by adding an additional 10 ns delay thereby temporally displacing the gate window from the coincidence peak. The recorded coincidences are then composed of detector dark counts and multi pair contributions only and were subtracted from the measured coincidences to calculate a corrected density matrix. The uncorrected values decrease from 0.94 at 0 km to 0.83 at 75 km. At 101 km, the negativity is higher at 0.88 due to lower losses in set II. When background counts are removed $E_{\mathcal{N}}$ decreases from 0.99 to 0.93 in the first 50 km then remaining constant up to 101 km.

4.2. Two-photon visibility

Although the tomography portrays the full information about the quantum state, in quantum communication applications like QKD only a subspace of measurement bases is used in practice. We therefore measured the visibility in the HV and the $+-$ basis for fiber lengths up to 101 km. The two-photon visibility (V) was calculated using the definition $V = \frac{Max-Min}{Max+Min}$, where Max is the maximal coincidence rate as obtained for parallel polarizer settings at Alice and Bob and Min is the coincidence rate at orthogonal settings.

The measured data points in Fig. 4(a) show the uncorrected visibilities (no background subtracted) of the HV and the $+-$ basis as a function of fiber length. We display the average of the two visibilities since any negative effect on the polarization induced by the fiber should affect both polarizations basis equally. Indeed, we found the difference of the two visibilities (HV , $+-$) to be less than 3%.

After the first spool, a decrease in visibility from 96.6% at the source to 93% is observed. The visibility remains approximately this value for transmission distances up to 60 km before decreasing steadily to 82.7% at 88 km. For the 101 km fiber we see yet a higher value of 88.6%,

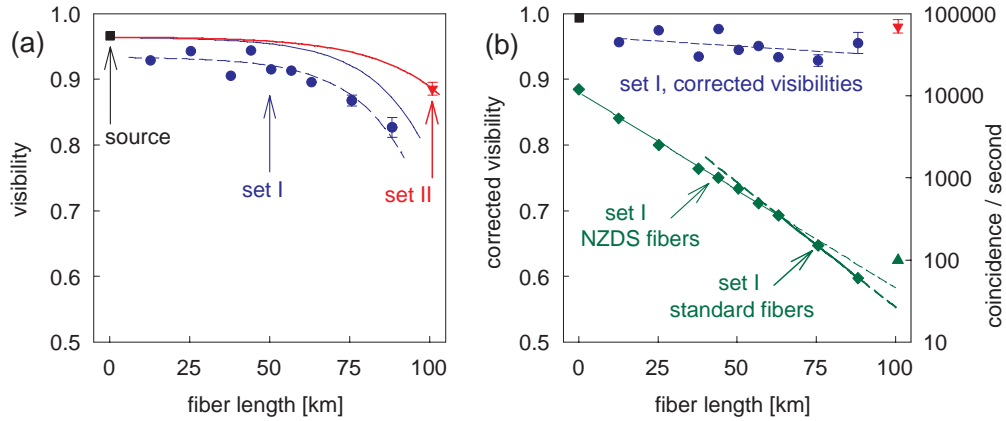


Fig. 4. (color online) (a) Uncorrected visibilities at the source (■), in fiber set I (●) and II (▼) measured at different fiber lengths. The solid curves represent model calculations (Eq.3) for set I and II. For the measured data of set I we observe a discrepancy of 3 to 5% (dashed curve) with the model, indicating additional depolarization in the fiber. (b) Corrected visibilities (background subtracted) at the source (■), in fiber set I (●) and set II (▼). Again, the fitted dashed line to set I indicates a decrease in visibility from 4% to 6% below the expected value. The measured coincidence count rates for set I (◆) and II (▲) are displayed on the right scale. The increased loss due to higher chromatic dispersion in the standard fibers (> 63 km) is clearly visible in the different slopes before and after 63 km.

because of the larger number of coincidences and hence greater ratio between coincidences and dark counts. The fluctuation seen in the data may in part be due to experimental error in compensating for the polarization drift or depolarizing effects in the fiber, like PMD. Error bars indicate the variance due to Poissonian statistics in the count rates. The upper plot in Fig. 4(b) shows the corrected visibility (V_{cor}), the same data as in Fig. 4(a) but with background counts removed. At the source (0 km), V_{cor} was measured to be 99.3%. For all distances measured with fiber set I, V_{cor} remains around 95%. Using the 101 km fiber we see an increase from 89% (uncorrected) to $V_{cor} = 98\%$.

Since such a simple background subtraction substantially improves the correlation for far distant data points, we therefore constructed a model to predict the reduction in the raw visibility V over the transmission length l based on dark counts, multi-pair emission and chromatic dispersion:

$$V(l) = \frac{(Max_0 - Min_0) T(l) F(l)}{((Max_0 + Min_0) F(l) + 2R_{acc}) T(l) + 2R_{dark}} \quad (3)$$

where Max_0 and Min_0 are the coincidence rates at 0 km, $T(l)$ is the measured transmission after length l , R_{acc} is the accidental coincidence count rate at 0 km (due to multi-pairs) and R_{dark} is the detector dark count rate. $T(l)^2$ terms for multi-pairs were omitted since their effect is less than 0.5% on the visibility. The dark count rate was measured by closing the fiber input port of the InGaAs detector but still triggering it with the Si-APD. Since R_{dark} is independent with transmission distance it will be the dominant factor in decreasing the visibility at large distances. $F(l)$ describes the effect of chromatic dispersion causing a broadening of the photon wavepacket which may eventually become wider than the detector gate window, leading to a decrease in Max and Min . $F(l)$ is calculated from $\int D(t) G(t, l) dt$, the overlap

between the detector response (gate window) $D(t)$ and the distance-dependent width of the gaussian wavepacket $G(t, l)$. Note that R_{acc} is not affected by chromatic dispersion. The parameters Max_0 , Min_0 , R_{acc} and R_{dark} were experimentally determined from measurements of the source. $T(l)$ and $F(l)$ were found from experimental characterization of the fibers.

All parameters in Eq. 3 were measured independently and the resulting curves for fiber set I and II are drawn in Fig. 4(a). The curves start at the measured visibility at the source, remaining constant up to about 60 km and then drop off due to detector dark counts. The prediction for fiber set II shows a slower decline due to higher transmission ($T(l)$) and lower chromatic dispersion ($F(l)$).

The comparison of the experimental data to our basic model leads to the conclusion that the decrease of visibility at larger distances can be explained predominantly by detector dark counts and chromatic dispersion effects and only a minor component is attributed to PMD of the optical fiber:

- The model predicts the measured point very accurately for set II, Fig. 4(a), implying that with this fiber there are no additional effects leading to a reduction of the visibility.
- For set I, the measured raw visibility, lies on average 3%-5% lower than the model curve. This difference indicates that depolarization effects are present in the fiber which are not covered by our model. However, the dashed guide-to-the-eye (offset with the model curve) implies almost no additional loss of coherence at longer lengths.
- This tendency can also be seen when studying the corrected visibilities in Fig. 4(b). After an initial drop in the corrected visibility to 96% (3% lower than at the source), only a small additional decrease of about 2% for the remaining 75 km of set I is observed. Similarly, for set II, a decrease of about 1.3% is observed for the whole 101 km transmission, giving an estimate of how much the fiber disturbs the polarization state.
- The stronger decrease for set I at shorter distances could be because the first spool of fiber might have been slightly damaged or these fibers have an exceptionally high PMD. Since PMD could not be directly measured we did not include its effects in our model. We do however think that this point still deserves further investigations and are planning further experiments using short polarization maintaining fibers to study the effects of PMD alone.

With the measured data, the performance of such a system for quantum key distribution is estimated as follows: Due to lower QE and a lossy polarization measurement at Bob, the local coincidence rate was decreased to ~ 12 kcounts/s. The measured coincidence rates are displayed in Fig. 4(b). The exponential decrease corresponds to a loss of 0.23 dB/km on average for set I and a smaller loss of 0.21 dB/km for set II. With the latter, a coincidence rate of 104 counts/s could still be detected after 101 km. The same sifted key rate is expected for QKD [2, 10], if four detectors are used. An average qubit error rate of 5.7% is estimated from the raw visibility. Ideal Entanglement based systems have been proven secure against individual attacks if the emission of multi-pairs is neglected [22]. Under these circumstances the privacy amplification results for the BB84 protocol can be applied. Including realistic error correction [23] and privacy amplification for individual attacks [24], a secure key rate of 35 bit/s could potentially be extracted after 101 km.

Finally, we can give an estimate from our model on the maximal distance for distributing entanglement in fibers. For this we assume a source with the same characteristics as presented here and a detector at Bob's side with a lower dark count rate together with the estimated 2% loss of visibility for every 100 km of fiber. We can neglect dispersion effects in this calculation

($F(l) = 1$) since smaller bandwidths can be achieved using longer crystals [8]. Superconducting single-photon detectors (SSPD) are currently the best choice for low noise detection in the telecom band. SSPDs have already been used for detection of entangled photons and exhibit a dark count rate of about 50 c/s (ungated) and a QE of 0.5% [25]. This would correspond to a total dark count rate of 0.0015 c/s for our experimental set-up and would allow the detection of quantum correlations without background subtraction up to 200 km. The total rate at this distance would however be in the order of one count in 100 seconds.

5. Conclusion

We have shown quantum polarization correlation between photon pairs after 101 km of optical fiber transmission without background subtraction, sufficient for secure QKD using commercially available fibers and detectors. Through measurements of the two-photon visibility and quantum state tomography we have observed only minor depolarization of the state caused by PMD of the optical fiber. Instead, the degree of observed quantum correlation is limited by detector dark counts, multi-pair emissions and chromatic dispersion. Modern fibers have a far smaller influence on the polarization state than previously thought, even at distances of up to 101 km and probably beyond this length.

We demonstrate that polarization encoding and this distribution method can readily be implemented as a QKD scheme. Moreover, polarization encoding provides more convenient control in photon-atom interactions and together with its observed robustness during optical fiber transmission makes polarization encoded qubits ideal for future long-distance quantum communication applications, like quantum repeater networks.

Acknowledgments

We would like to thank Sebastien Sauge and Daniel Ljunggren (KTH, Kista) for the intense and ongoing discussions on generation and distribution of entanglement. In addition we like to thank Reinhard Binder from Mattig-Schauer and David Peckham from OFS for the loan of the 101 km of TrueWave© optical fiber. We also acknowledge the financial support from Austrian Research Centers GmbH, Austrian Science Fund FWF (SFB15) and Stadt Wien. This work was supported by the European Commission through the integrated projects SECOQC (Contract No. IST-2003-506813) and QAP (No. 015846).